Microtubules and vesicles under controlled tension

D. Kuchnir Fygenson,[1] M. Elbaum,[2,*] B. Shraiman,[3] and A. Libchaber,[1,2]
[1]*The Center for Studies in Physics and Biology, Rockefeller University, 1230 York Ave., New York, New York 10021*
[2]*NEC Research Institute, 4 Independence Way, Princeton, New Jersey 08540*
[3]*AT&T Bell Laboratories, 600 Mountain Avenue, Murray Hill, New Jersey 07974*
(Received 14 May 1996)

Microtubules trapped inside cell-sized vesicles ($\sim$10-μm diameter) define shapes reminiscent of living cells. In this work, three configurations are studied: an individual microtubule, a linear bundle, and a circular band. Mechanical properties are probed by varying the vesicle membrane tension using micropipet aspiration. Quantitative results include measurements of the persistence length of a single microtubule, 6.3 ± 2.4 mm, and the stretching modulus of the vesicle membrane, $k_s \geqslant 140$ erg/cm^2. The number of microtubules in a typical bundle is $\sim$100, and the total length in a typical band is $\sim$0.5 cm. A tension-induced first-order transition from linear bundle to circular band is observed and modeled. The loss of stability of the bent bundle is associated with a saddle-node bifurcation. [S1063-651X(97)11201-6]

PACS number(s): 87.45.$-$k

I. INTRODUCTION

One organizing principle in biology is that form follows function. At the cellular level, this means that morphology both reflects and constrains cellular activity. Thus an investigation into cellular architecture and mechanics may be an important step for understanding biological design.

Cellular architecture has one universal theme: phospholipid bilayers [1]. These are membranes that define the boundaries of and within the cell [2,3]. Mechanically, they are two-dimensional liquids [4] (thickness $\sim$5 nm). Their liquid nature means that, in equilibrium, tension is uniform throughout the bilayer just as pressure is uniform in a three-dimensional fluid. These membranes cannot support mechanical shear but they resist stretching and bending, with elastic constants $k_{\text{stretch}} \sim 10^7 k_B T/\mu\text{m}^2$ and $k_{\text{bend}} \sim 15 k_B T$, respectively [5].

As a two-dimensional structure, a phospholipid bilayer is able to separate three-dimensional space into distinct regions. Yet, it cannot establish unique spatial relationships between or within those regions. For this next level of organization, a one-dimensional structure is required.

The microtubule is just such a one-dimensional structure, and nearly as common in cells as the phospholipid bilayer. Microtubules are cylindrical aggregates (diameter $\sim$25 nm) of the protein tubulin, best known for switching stochastically between episodes of aggregation and dissolution (growth and shortening), a behavior called dynamic instability [6]. Microtubules are also unique among the protein polymers for their ability to individually apply an extensive force at a significant distance on the cellular scale. In other words, they can push at long range. Ambient Brownian forces, of order pN ($k_B T$ over the typical macromolecular dimension $\sim$1 nm), are not strong enough to buckle microtubules shorter than 10 μm.

Certain characteristic cell morphologies seem to depend upon the interaction of microtubules with cell membranes. For example, the oblate shape of avian or amphibian red blood cells develops concomitantly with a circular band of microtubules [7], and the long, thin extensions of nerve cells grow in concert with linear bundles of microtubules [8]. The basic physical interaction between microtubules and a membrane that confines them must underlie the selection of these geometries.

This work is a study of the simplest interaction between microtubules and membranes. Their delicate mechanics is probed by a combination of differential interference contrast (DIC) microscopy and micropipet aspiration [9]. Cell-sized vesicles ($\sim$10-μm diameter) containing spontaneously nucleated microtubules are used, as in earlier work [10,11]. The vesicles assume shapes which resemble those of the real cells described above. Relevant elastic constants, the microtubule persistence length, and the membrane stretching modulus are measured, and the overall structural response of the ensemble to increased membrane tension is described. The experiments reveal a sharp transition between elongated and circular morphologies which is understood in terms of mechanical constraints imposed by both microtubule and membrane.

II. METHODS

A. Sample preparation

The sample is a solution of giant unilamellar vesicles containing purified tubulin under conditions that promote its assembly into microtubules. The key chemical concerns are to ensure the fluid state of the bilayer, to form $\sim$10-micrometer-diameter vesicles of single bilayers in ionic buffer, and to avoid nonspecific binding between tubulin and lipid. The key physical concerns are to control the osmotic conditions across the membrane, to enhance the optical contrast of the vesicles, and to sediment the vesicles for observation on an inverted microscope.

Vesicles are made of two synthetic phospholipids, DOPC (dioleoyl phosphatidyl choline) and DOPS (dioleoyl phosphatidyl serine), in a 70:30 ratio. With two monounsaturated

*Present address: Department of Materials and Interfaces, Weizmann Institute of Sciences, Rehovot, 76100 Israel.

carbon chains, 18 carbons long, these lipids have a gel-sol transition temperature well below 0 °C. The mixture of net neutral (choline) and negatively charged (serine) head groups stabilizes the bilayers in ionic solution and inhibits binding with the negatively charged tubulin or microtubules.

The lipids are purchased in chloroform solution (Avanti Polar Lipids). The DOPC/DOPS mixture is deposited onto a roughened teflon disk on the bottom of a glass vial, and the chloroform is allowed to evaporate under a fume hood. The vials are then placed in a vacuum dessicator for at least 1 h. The dry lipid is hydrated with vapor for 1 h in a warm (55 °C), water-saturated atmosphere. A microtubule-assembly buffer (100-mM Pipes acid, 2-mM $MgSO_4$, and 1-mM EGTA, pH 6.90 by NaOH titration) is added to the vial, and it is returned to the warm, humid atmosphere for another 4–6 hours. A cloud of lipid rises from the teflon. It contains mainly large, loosely packed ''onions'' of bilayers. The cloud is extracted with a pipet, along with about 400 μl of solution, and vortexed gently to homogenize. This is the lipid stock [12].

Tubulin is purified (>99.99% by weight) from bovine brain according to a published protocol [13,14], and stored in liquid nitrogen. Concentrated tubulin (typically 10–15 μl at 145 μM) is mixed with lipid stock and GTP to create a final volume of ~50 μl, with ~30-μM tubulin and 1-mM GTP. The mixture is flash-frozen in liquid nitrogen and allowed to thaw slowly on ice (4 °C). Holding on ice prevents spontaneous nucleation of microtubules [15]. Freezing ruptures the onions, fragmenting bilayers which then close upon themselves, entrapping the tubulin and the surrounding solution [16]. This is the sample stock. It is prepared fresh immediately prior to each observation, and used within 1 h.

The sample stock is diluted into warm, 150-mM NaCl solution on the microscope. This solution has ~20% greater osmolarity than the one inside the vesicles [17] to increase the surface to volume ratio. Also, the contrast between NaCl outside and Na-Pipes inside the vesicles creates a refractive index mismatch which improves their visibility, and a density mismatch which causes them to sediment. Otherwise the vesicles remain largely beyond the focal range of the microscope objective.

B. Apparatus

The apparatus consists of four major elements: the sample cell and a micropipet pressure control system (Fig. 1), the microscope, and optical tweezers. The sample cell is simply a $\frac{1}{8}''\times\frac{7}{8}''$ *o* ring sealed onto a glass cover slip (thickness ~0.17 mm) with paraffin wax (Fig. 1). On the bottom of the cell lies a strip of tantalum foil 25 μm thick. This serves as a ledge for the micropipet, which must enter the cell at an angle (~20%). By lowering the micropipet onto the foil just behind the tip, it can be bent to horizontal, so that its length near the tip lies in focus. The temperature of the sample is maintained by fluid circulating through a collar around the oil-coupled microscope objective. The cell contains ~350 μl of solution covered with a layer of mineral oil [18]. The mineral oil is added last (after sample stock and micropipet) to prevent evaporation during the experiment.

The system is built around an inverted microscope (Zeiss Axiovert 35) equipped for DIC using a 63×/1.40 NA Plan Apochromat oil-immersion objective and an air-coupled 0.63 NA condenser (NA stands for numerical aperture). The low NA condenser was chosen for its large working distance (7 mm), which allows access to the micropipet. The associated lack of light is compensated for by using a 75 W Xe short-arc lamp (Opti-Quip), coupled through a mode-scrambling optical fiber (Technical Video) in critical illumination (rather than the standard Koehler) and a nonabsorbing Glan-Thompson prism in place of a film polarizer in the illumination path. The microscope image is recorded through a Hamamatsu Newvicon video camera and taped in S-VHS format.

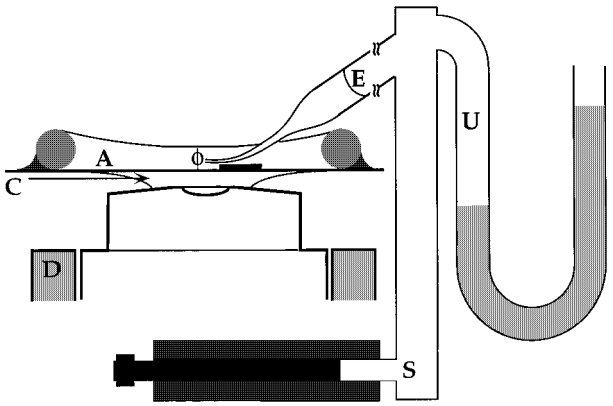

FIG. 1. The sample setup: (*A*) fluid medium covered with mineral oil. (*B*) *O*-ring, $\frac{1}{8}''\times\frac{7}{8}''$, sealed with paraffin to a glass cover slip (No. 1). (*C*) oil-immersed microscope objective (63×/1.40 NA. Plan Apochromat). Total magnification to camera 252× (not shown). (*D*) objective water jacket for temperature regulation. (*E*) Micropipet with meniscus. The micropipet is mounted in a three-axis hydraulic micromanipulator, and introduced from the side at an angle of 20°. A strip of tantalum foil, 25 μm thick, lies on the bottom of the cell near the center. When a vesicle is chosen and aspirated, the pipet is lowered onto the foil some distance behind the tip, so as to bring its end into focus. The pressure control system: (*S*) syringes and a 10-ml thumbwheel-driven pipettor (not shown) create a negative displacement ΔV against a gas ballast $V=500$ ml, and produce a pressure change determined by the ratio $\Delta V/V$. Absolute pressure is referenced to atmospheric through a water-filled *U* tube (*U*), and transmitted to the micropipet barrel. All tubing connections are made of hard-walled plastic, the gas ballast is thermally insulated, and the manometer is thermally regulated.

Optical tweezers are used to orient and organize the sedimented vesicles. Laser light enters the objective via a dichroic mirror mounted in the epifluorescence filter cube. Two laser sources are available: 488 nm (Lexel 90-2, Ar-ion laser, 2 W) and 830 nm (SDL 5432, IR single-mode diode, 200 mW). The blue light interacts strongly with the vesicles, causing them to invaginate and form tense spheres. It also cuts the microtubules. The infrared laser, at reduced power (80 mW), manipulates the vesicles and microtubules unharmed.

The heart of the measurement is the controlled application of suction through a micropipet, and a simultaneous determination of the membrane position in the pipet. The pressure control system (Fig. 1) is based on a temperature-stabilized capacitance manometer (MKS Baratron 220) with a full-scale range of 10-cm H_2O (~10 000 dyn/cm^2). The manom-

eter output is read by a digital voltmeter (1 V=1 cm H_2O), and inserted into the video image using a screen splitter (Ikegami). Suction is applied by increasing the closed volume behind the micropipet with a syringe. The pressure stability depends critically on thermal insulation, the ballast volume, rigid wall interconnection tubing, low backlash in the syringe motion, and the absence of air bubbles in the pressure lines. The effective zero pressure is calibrated for each run to correct for the meniscus inside the micropipet. This is a delicate part of the procedure.

The micropipet itself is drawn from a borosilicate glass capillary tube (1 mm o.d., 0.75 mm i.d.) using a programmable puller (Sutter Instrument Co.). The long, narrow tip is cut to the desired diameter under a stereomicroscope by thermal shock from a hot tantalum filament [19]. Then the micropipet is backfilled with the 150-mM NaCl solution using a quartz-kapton filling needle (World Precision Instruments) and mounted on a three-axis hydraulic micromanipulator (Soma Scientific) that is anchored to the microscope's tilting illumination pillar. The micropipet holder includes a tantalum wire which makes contact to the fluid in the pipet, and is grounded to eliminate static charge in the sample. After each run, the inner diameter of the pipet is recorded by imaging the pipet immersed in refractive-index matched oil [Fig. 2(a)]. Typical inner diameters ranged from 3 to 5 μm. The extent of membrane intrusion into the pipet is measured as the peak-to-peak distance in an intensity profile along the pipet axis [Fig. 2(b)]. Distance between microtubule ends is measured in a similar manner. Using this method, the resolution in relative displacements is limited by pixel size, ~ 0.08 μm.

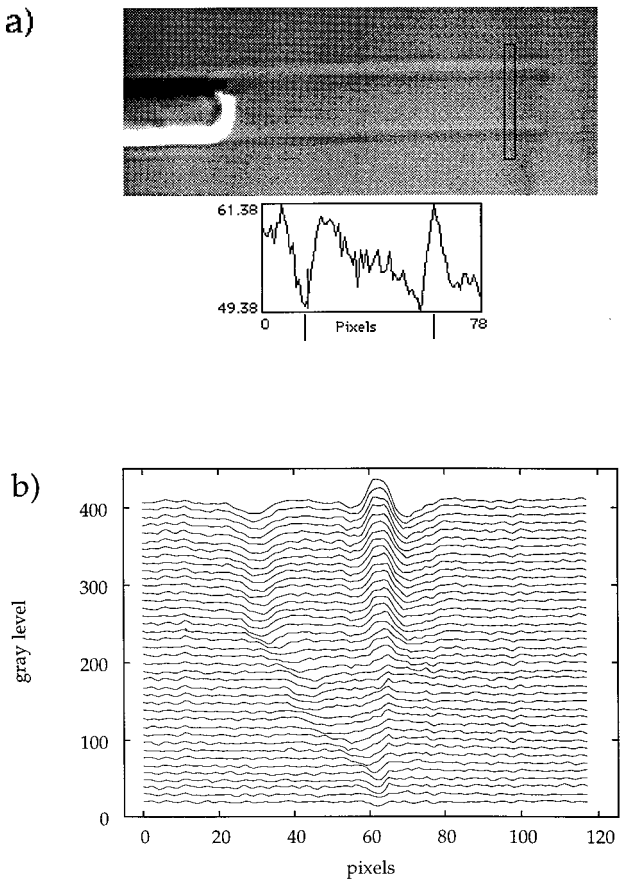

FIG. 2. The micropipet immersed in index-matched oil. The inner diameter is measured as the distance between two peaks in the gray scale profile (inset) along a line perpendicular to the pipet axis (6 μm long). The water-oil meniscus is clearly visible. Scale: 12.8 pixels/μm. (b) Position of the membrane inside the micropipet (Fig. 4). Each trace plots the mean gray scale in the image along a line (five pixels wide) that lies on the central axis of the pipet. Suction pressure increases slowly, but not steadily in time. One trace is taken every 0.2 s. The end of the micropipet is indicated by the maximum, and the membrane intrusion by the minimum. In the bottom trace the membrane is at the edge of the micropipet. In the top trace the membrane is about 2.7 μm in from the edge.

III. RESULTS

A. On shapes and scales

As soon as sample stock is introduced to the cell, microtubules begin nucleating spontaneously within the vesicles. The microtubules grow as the vesicles sediment. By the time they settle, the vesicles are distorted.

The vesicle shapes fall into two classes depending on whether the microtubules are straight or buckled (Fig. 3). In the first class, the microtubules impose their linear form on the vesicle, protruding *without piercing the membrane* [20]. The vesicle extends a pair of narrow tubes about the microtubule extremities while maintaining a roughly spherical central portion, the final shape resembles the Greek letter ϕ in profile. In the second class, the vesicle imposes its circular geometry on the microtubules, bending them *without breaking* [21]. The microtubules form a circular band and exaggerate the vesicle circumference in one plane, creating a sharp-edged, discoid shape.

Other shapes, intermediates or combinations of the two major classes, are also seen. The evolution of vesicle shape during microtubule growth and bending is documented and explained elsewhere [22].

Before entering a quantitative investigation of the mechanics of microtubules in vesicles, let us emphasize the natural scales of length, energy, and force in our experiment. Vesicle membranes are 5 nm thick. The vesicles we observe are between 5 and 10 μm in diameter. Microtubules are 25 nm in diameter. The microtubules we observe reach tens of micrometers in length. Our typical concentration of tubulin, 30 μM, corresponds to 18 000 molecules/μm^3. Since 1 μm of microtubule contains 1750 molecules of tubulin [23], this corresponds to over 10 μm of microtubule from every μm^3 of solution and a maximum of several millimeters of microtubule possible in a typical vesicle.

The relevant energy scale is $k_BT \sim 4\times10^{-14}$ erg. The energy of binding a tubulin molecule to the microtubule is only a few times greater [24]. The scale of force that dominates biological mechanics is several k_BT/nm, or about ten pN. When applied over the typical cross section of a micropipet, 10 μm^2, this specifies a pressure of 10 dyn/cm^2=1 μ atm =0.1 mm H_2O, the latter of which is the natural unit for the pressure control system used in these experiments.

B. Single microtubule

To determine the bending rigidity of a microtubule, a vesicle deformed by a single microtubule was subjected to

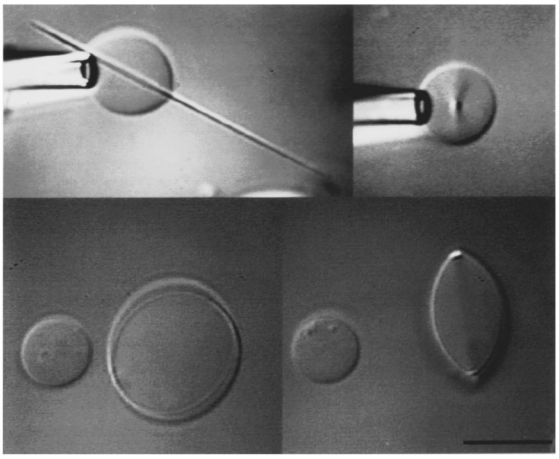

FIG. 3. The two classes of vesicle shapes. Scale bar at bottom right: 10 μm. Above: a ϕ shape in two perspectives. Left: nearly horizontal. Right: turned end-up in the micropipet. Below: a discoid shape in two perspectives. Left: nearly horizontal. Right: turned end-up by an infrared optical tweezer.

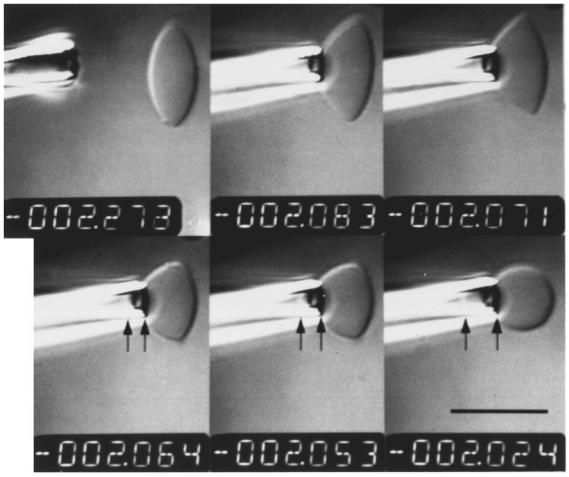

FIG. 4. Six images of a single microtubule buckling as micropipet suction increases the tension of the confining membrane. Note the changing position of the membrane inside the pipet, indicated by the arrows. The number in the bottom left of each image is the suction pressure in units of cm H_2O=980 dyn/cm^2. Zero pressure is at -2.074. The pipet radius is 1.5 μm. Scale bar: 10 μm.

micropipet aspiration. The vesicle, originally ϕ shaped, was formed with 25 μM tubulin at 30 °C. The number of microtubules inside was reduced upon lowering the temperature to 27 °C. (Low temperatures cause microtubules to disassemble and eventually disappear [14].) Eventually, the vesicle became a pointed prolate (football) with a long axis of 9 μm defined by a single microtubule [25]. This configuration persisted for about 10 min, until the lone microtubule shortened suddenly to less than the vesicle diameter, 7 μm. Meanwhile, the vesicle was subjected to suction from the micropipet. During any single pressure sweep ($\sim$10 s) the microtubule did not change significantly in length [26].

Figure 4 is a sequence of images of the vesicle deforming and the microtubule buckling as the suction pressure increases. In the lower three images, the membrane is visible inside the micropipet (see arrows). Figure 5 is a plot of the suction pressure P vs the extent of the membrane intrusion X, and vs the distance between the microtubule endpoints, L'. Initially the microtubule resists compression, and work goes into damping long-wavelength curvature fluctuations of the membrane (i.e., tightening the vesicle). At a suction of 11 dyn/cm^2, the microtubule buckles. The transition appears continuous on the video. As the suction increases, the microtubule bends smoothly. Eventually, the vesicle becomes a sphere. Increasing suction must then change the radius of the sphere to affect the microtubule. Because the vesicle volume is constant [27], work goes instead into increasing the membrane area. For the very low level of tension applied (of order 10^{-3} erg/cm^2), entropic fluctuations are the main source of membrane area [28,29].

The result is a direct, active mechanical measurement of the bending stiffness of the microtubule. The elastic energy stored in the microtubule is equal to the work done displacing the vesicle volume into the pipet as the microtubule bends. The latter is simply

$$U=\int P\, dV=A\int P\, dX, \tag{1}$$

where V is the volume of the intrusion, and A is the cross-sectional area of the micropipet. (We ignore any change in mean membrane curvature as the microtubule bends, since the associated energy is several orders of magnitude less than the elastic energy in the microtubule.) The mechanical energy stored in the microtubule is proportional to the square of the mean curvature, H, integrated over its length,

$$\tfrac{1}{2}EI\int H^2 ds=\tfrac{1}{2}EI\int y''^2\sqrt{1+y'^2}\,dx, \tag{2}$$

where E is Young's modulus, I is the moment of inertia, and $y(x)$ describes the shape of the microtubule. The product EI is known as the bending stiffness. For small deformation, the first derivative y' is negligible, and the shape of the micro-

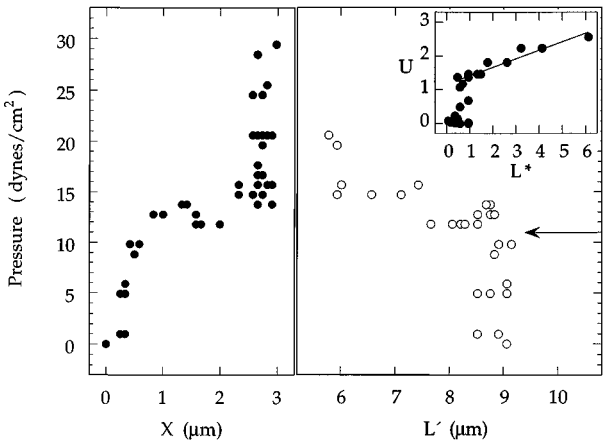

FIG. 5. The single microtubule case: Suction pressure vs intrusion of the membrane into the micropipet X, and vs the end to end distance of the microtubule, L'. The arrow indicates critical buckling. The inset shows the work done on the vesicle, $U=\int P\, dV = A\int P\, dX$ (pipet cross section A=9.1 μm^2) in units of 10^{-10} erg vs $L^*=(L\text{-}L')/L'^2$ in units of 10^2 cm^{-1}. The slope yields a measure of the bending modulus, $EI=2.6\times10^{-14}$ dyn cm^2.

tubule is described by $y(x)=(2/\pi)\sqrt{L'(L-L')}\sin(\pi x/L')$. The mechanical energy stored in the microtubule is then

$$\tfrac{1}{2}EI\int_0^{L'} y''^2 dx=\frac{\pi^2 EI(L-L')}{L'^2}=\pi^2 EIL^*, \qquad (3)$$

where L is the unbent length of the microtubule and L^* is defined for notational convenience. A plot of U vs L^* is a straight line, as shown in the inset of Fig. 5, with a slope proportional to the bending stiffness. This measurement gives $EI=(2.6\pm1.0)\times10^{-14}$ dyn cm^2 (persistence length [30] $L_p=6.3\times2.4$ mm) which lies in the range of other recent measurements [31–35]: $EI=(0.85–6.2)\times10^{-14}$ dyn cm^2.

C. Linear bundle of microtubules: bending

When the same experiment is repeated on a ϕ-shaped vesicle that contains a bundle of microtubules, the strength and size of the bundle can be extracted from the critical force for buckling,

$$\mathcal{F}_c=\frac{\pi^2 EI_{\text{bundle}}}{L^2}, \qquad (4)$$

where L is the length of the bundle.

The analysis is complicated because the force on the bundle depends on the radius r of the arms of the ϕ shape, which is not resolved under the microscope (i.e., $r<0.25$ μm). A self-consistent argument can be constructed as follows: estimate the number of microtubules in the bundle from the conditions in which it formed (i.e., temperature, tubulin concentration); calculate their close-packed radius; use this radius to deduce the force at critical buckling; and check if the apparent stiffness corresponds to the combined stiffness of the estimated number of microtubules.

We consider two ϕ-shaped vesicles, similar in length but different in size, shown in Figs. 6 and 7. The first (Fig. 6) was formed at $T=37$ °C, with $C=50$ μM tubulin [36] and had a volume $V=125$ μm^3. At this temperature, an estimated 6-μM tubulin concentration remains in solution after polymerization is complete [37]. Thus approximately 1.9 mm of microtubule was assembled. Since this vesicle contained a bundle 32.5 μm long, it is estimated that there were 58 microtubules inside. Close packed (packing fraction 0.907), 58 microtubules make a bundle 0.09 μm in radius. For the second vesicle (Fig. 7), ($T=37$ °C, $C=44$ μM, $V=500$ μm^3, and $L=38$ μm) a similar analysis yields an estimated 170 microtubules in a 0.16-μm-radius bundle.

These radii can be used to estimate the force applied on the microtubule ends, $\mathcal{F}=2\pi r\tau$, by the tension in the membrane, τ. Since the central portion of the vesicle becomes spherical before the bundle buckles, the analysis of Kwok and Evans [9], applies and the tension in the membrane is approximately

$$\tau=\frac{PR_p}{2(1-R_p/R_0)}, \qquad (5)$$

where P is the suction pressure, R_p is the radius of the micropipet, and R_0 is the radius of the spherical portion of the vesicle. The error introduced by neglecting the arms of the phi shape is of the order of r/R_0, ~4%.

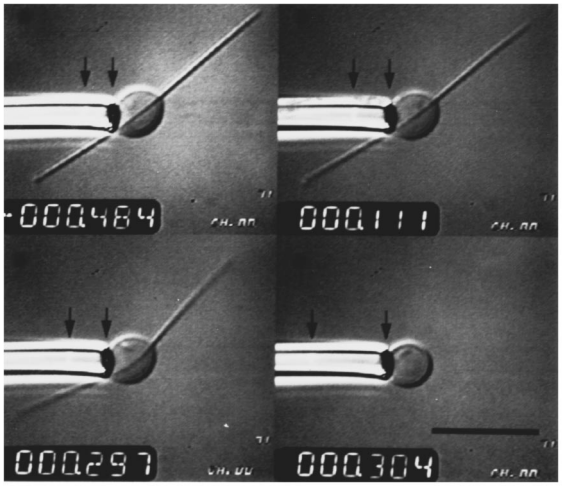

FIG. 6. Buckling and collapse of a microtubule bundle. A ϕ shape with a relatively small central portion ($R/L\sim0.1$). 42-μM tubulin and 37 °C. Zero suction pressure at -0.71-cm H_2O. The bundle is slightly buckled in the first image. In the next two images, the bend increases very slowly as the suction rises. In the fourth image, the bundle has collapsed into a ring lining an inner circumference of the vesicle and the membrane has moved into the pipet (arrows). A large pressure change is needed to transform a ϕ shape to a spherical vesicle. Scale bar: 10 μm.

The first bundle (Fig. 6: $r=0.10$ μm, $R_0=2.5$ μm, and $R_p=1.5$ μm) began to buckle when the suction was 125 dyn/cm^2. Thus the critical buckling force [Eq. (4)] was 15 pN, corresponding to a bending stiffness $EI_{\text{bundle}}=1.6\times10^{-12}$ dyn cm^2. Dividing this by the bending stiffness of a single microtubule measured above, $EI_{\text{single}}=2.6\times10^{-14}$ dyn cm^2, gives the number of microtubules in the bundle, 62, consistent with the number calculated earlier. The second vesicle, (Fig. 7: $r=0.18$ μm, $R_0=4.8$ μm, and $R_p=1.6$ μm) buckled with a suction of 240 dyn cm^2. The critical buckling force was 33 pN and, again, $EI_{\text{bundle}}=4.8\times10^{-12}$

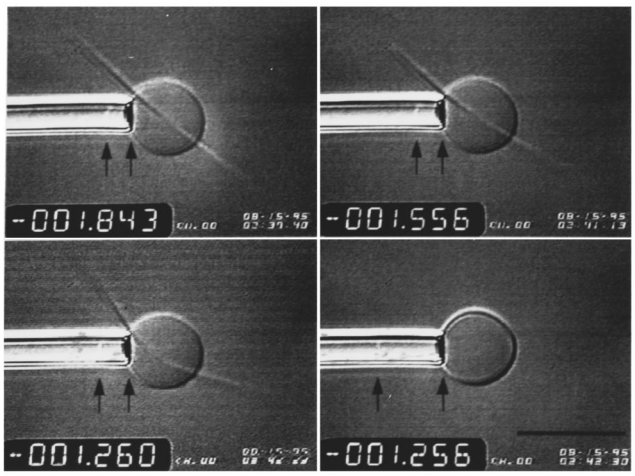

FIG. 7. Buckling and collapse of a microtubule bundle. A ϕ shape with a relatively large central portion ($R/L\sim0.3$). 37-μM tubulin and 37 °C. Zero suction pressure at -2.160-cm H_2O. The evolution is similar to Fig. 6. Scale bar: 10 μm.

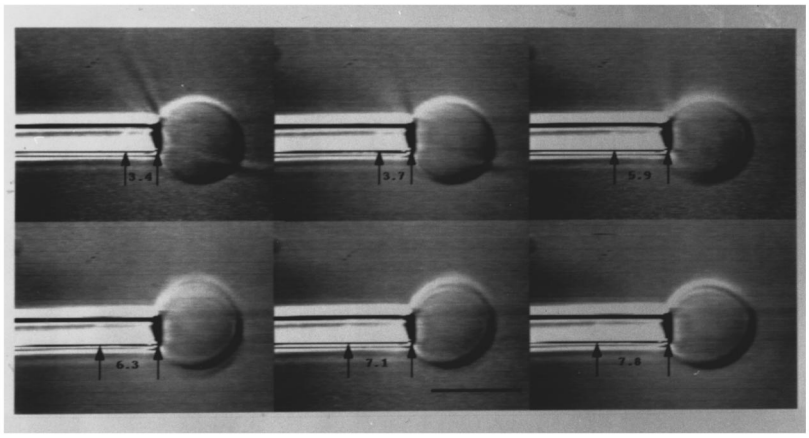

FIG. 8. Collapse of the bundle shown in Figure 7. 0.03 s between frames. The evolution of the collapse is clearly shown by the intrusion of the membrane indicated by the arrows and labeled in micrometers. The plane containing the bundle is at a steep angle with respect to the focal plane. Scale bar: 10 μm.

dyn cm^2=185 EI_{single} again consistent with the estimated number of microtubules [38].

Based on this argument, it appears that the bending rigidity of the bundle is simply the sum of the bending rigidities of the individual microtubules. Were there a large attractive interaction, or significant static friction, between bundled microtubules, it would have been noticeably more resistant to buckling. The successful estimation of the membrane radius r supports the assumption that, under tension, the lipid membrane is in close contact with the microtubule bundle.

D. Linear bundle of microtubules: collapse

Beyond critical buckling, the bent ϕ shape is surprisingly stable. Selected images are shown in Figs. 6 and 7. Though the suction pressure more than doubles, the bending increases only slightly. Suddenly, at a suction 4–10 times that which initially caused buckling, stability is lost, and the bundle collapses into a circular band. Figure 8 is a sequence of images from the collapse of the vesicle in Fig. 7, which lasts about 0.2 s. Figure 9 illustrates the discontinuous nature of the transition by tracing the hysteresis of the membrane intrusion into the pipet.

To understand the unexpected stability of the slightly bent bundle, consider the equilibrium of the buckled microtubule. The forces acting on the microtubule are generated by the fluid membrane, and are necessarily normal to its surface. There is a longitudinal force component $f_{\|}=2\pi r\tau$ applied at the tip of the microtubule, and a transverse force component $f_{\perp}$ applied where the membrane loses contact with the microtubule (Fig. 10, inset). The latter force is due to the asymmetry of the contact line between the membrane and the tubule and depends on the angle δ between the microtubule axis and the plane of the membrane, but the exact form of the dependence is not known. It is clear, however, that the scale of $f_{\perp}$ is set by $f_{\|}$, and that, for small angles, $f_{\perp}$ is proportional to δ. As δ increases, the contact line, an ellipse, increases in eccentricity, degenerating into two parallel lines along the microtubule axis when $\delta=\pi/2$, at which point $f_{\perp}$ diverges. This behavior is captured by a simple model

$$f_{\perp}=\frac{f_{\|}}{A}\tan\delta, \tag{6}$$

where A is an unknown dimensionless parameter.

The conditions for the force equilibrium are determined by the geometry of the vesicle. The microtubule extremities remain unbent in the buckled state because the applied force is strictly longitudinal. Bending starts at the point where the transverse component $f_{\perp}$ is applied. Force balance along the $\hat{z}$ axis dictates that

$$f_{\perp}\cos\beta=f_{\|}\sin\beta \tag{7}$$

which, together with Eq. (6), gives

$$\tan\delta=A\tan\beta. \tag{8}$$

The $\hat{x}$ component of the force exerted on the microtubule by the membrane, $\mathcal{F}$, is

$$\mathcal{F}=f_{\perp}\sin\beta+f_{\|}\cos\beta=\frac{f_{\|}}{\cos\beta}, \tag{9}$$

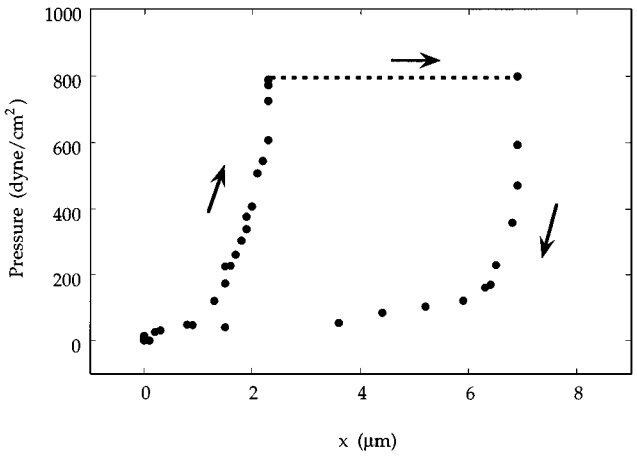

FIG. 9. The hysteresis of collapse. A plot of pressure vs membrane intrusion into the pipet, X. Arrows indicate the time course. At low suction the displacement is large as membrane fluctuations are damped. At higher suction the microtubule bundle supports the membrane until it collapses and the membrane leaps into the pipet (dotted line). Releasing the pressure, the slope is reduced as the elasticity of the bent microtubules is felt.

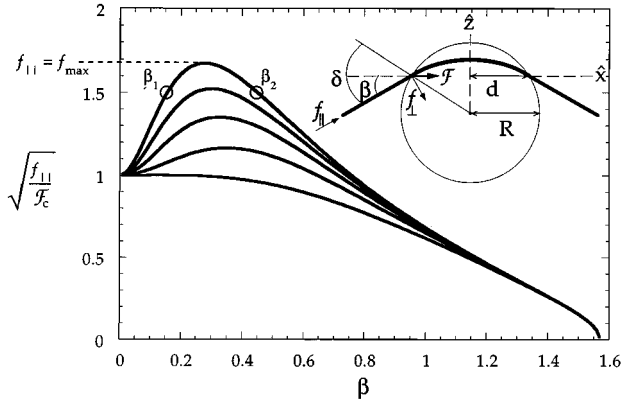

FIG. 10. Plot of $\sqrt{f_{\|}/\mathcal{F}_c}$ vs β for different values of the parameter A. The lowest curve corresponds to $A=2$. The four others correspond to $A=4$, 6, 8, and 10. β_1 is the stable, small angle solution and β_2 is the unstable, large angle solution. β is measured in radians. No stable solution exists for $f_{\|}>f_{\max}$. *Inset*: Schematic of forces acting on a buckling microtubule in a ϕ-shaped vesicle. $f_{\|}$ is the longitudinal force on the ends of the microtubule, $f_{\perp}$ is the perpendicular force, and $\mathcal{F}$ is the force balanced by the elasticity of the buckled region. β is the angle between the microtubule extremities and the line connecting the end points of the buckled region. δ is the angle of the microtubule extremities with the radius of the vesicle.

and is balanced by the microtubule rigidity. With the geometry of the bent microtubule parametrized by $d=R\cos(\delta-\beta)$ and the angle β, as defined in the inset of Fig. 10, we find [37]

$$\mathcal{F}=\frac{EI}{2d^2}\left[\int_0^{\alpha}\frac{\cos\phi}{\sqrt{\cos\phi-\cos\beta}}\,d\phi\right]^2 \tag{10}$$

Combining Eqs. (8), (9), and (10) yields

$$\left(\frac{f_{\|}}{\mathcal{F}_c}\right)^{1/2}=\frac{\sqrt{2}}{\pi}\,\frac{\int_0^{\alpha}\frac{\cos\phi}{\sqrt{\cos\phi-\cos\alpha}}\,d\phi}{\cos[\tan^{-1}(A\tan\beta)-\beta]}, \tag{11}$$

with $\mathcal{F}_c\equiv=\pi^2EI/4R^2$, the critical buckling force for a microtubule of length $2R$. Equation (11) implicitly gives the bending angle β as a function of $f_{\|}$, and hence of the tension in the membrane. A graphical solution of Eq. (11) is shown in Fig. 10 for various values of the transverse force parameter A. The large angle branch of the solution $\beta_2(f_{\|})$ is presumed unstable. The stable buckled state $\beta_1(f_{\|})$ exists for $\mathcal{F}_c<f_{\|}<f_{\max}$, where $f_{\max}$ (which depends on A) corresponds to a saddle node bifurcation. When $f_{\|}=f_{\max}$, the stable and unstable branches of the solution collide. Beyond, there is no stable solution—the bundle collapses.

E. Circular band of microtubules

After collapse, a ϕ-shaped vesicle is left, with a circular band of microtubules which gives it a discoid shape. A discoid shape may also arise directly when microtubules buckle individually as they span the vesicle diameter. In either case, under aspiration the microtubules slip past one another, and the band behaves like a circular spring.

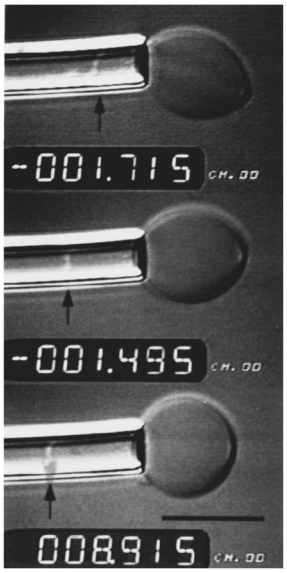

FIG. 11. Three images in the aspiration of a discoid shape. Note that the microtubule bundle is clearly visible in the first image. In the other two images it has rotated into the focal plane. The arrow indicates the intrusion of the membrane. Zero suction at −1.758. Scale bar: 10 μm.

Figure 11 shows three images of a discoid vesicle under aspiration. At the lowest suction pressure, the vesicle hangs out of the micropipet at an angle. For pressures below 1500 dyn/cm^2 (below the dashed line in Fig. 12), the membrane is drawn into the micropipet, and the radius of the band decreases. Similar suction pressures were applied to bend mi-

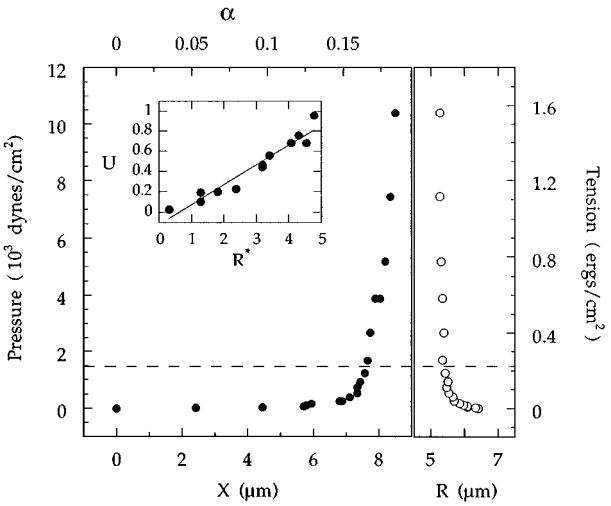

FIG. 12. The case of a microtubule band: Suction pressure vs intrusion of the membrane into the micropipet X, and vs the radius of the microtubule band, R. The inset uses the data from below the dashed line, and plots the work done on the vesicle, $U=\int P\,dV=A\int P\,dX$ (pipet cross section $A=9.1\ \mu$m^2) in units of 10^{-7} erg vs $R^*=\frac{1}{2}(R_f^{-2}-R_t^{-2})$ in units of 10^5 cm^{-2}. The slope in the inset yields a measure of the bending modulus for the band, $EI=4.4\times10^{-14}$ dyn cm^2. The three points at highest pressure measure the stretching modulus of the membrane. Using the right and upper axes, membrane tension τ, and area dilation α, one finds a slope $k_s=\tau/\alpha=140$ erg/cm^2. Conditions: 30-μM tubulin, 37 °C.

crotubule bundles (Sec. III C). At higher suction (above the dashed line), the vesicle is spherical, and its radius is nearly constant. Work goes into stretching the membrane rather than bending the microtubules. Thus the energy in the microtubule band does not change, and one measures the elastic property of the membrane alone.

Figure 12 is a plot of pressure P vs membrane intrusion X, and vs band radius R_b. Below the dashed line, the analysis parallels that of the single microtubule (Sec. III B). The elasticity of the band is derived by equating the work done on the membrane to the work done contracting the band,

$$U=\int P\ dV=\tfrac{1}{2}EIL(R_f^{-2}-R_i^{-2})=\tfrac{1}{2}EILR^*, \qquad (12)$$

where, the product EI is the bending stiffness of a microtubule (Sec. III B), L is now the total length of microtubule in the band, R_i and R_f are the band radii at the initial and final pressures, and R^* is defined for notational convenience. The inset to Fig. 12 is a plot of U vs R^*. The slope is the product $EIL=1.9\times10^{-14}$ dyn cm^3. The conditions of formation of the vesicle ($T=37$ °C, $C=30$ μM, and $V=800$ μm^3) yield an estimate of $L=6.7$ mm. Thus $EI=2.8\times10^{-14}$ dyn cm^2, which is consistent with the measurements described above for a single microtubule.

Above the dashed line, the analysis of membrane elasticity follows that of Kwok and Evans [9]. The membrane tension τ relates directly to the suction pressure P [Eq. (5)]. The distance of membrane intrusion, X, determines the fractional change in area, α, of the membrane:

$$\alpha=\frac{\Delta A}{A}=\frac{1}{2}\left[\left(\frac{R_p}{R_0}\right)^2-\left(\frac{R_p}{R_0}\right)^3\right]\frac{X}{R_p}. \qquad (13)$$

τ and α are displayed on the right and upper axes in Fig. 12 using the values $R_p=1.9$ μm and $R_0=5.3$ μm. The slope defined by the three points at the highest pressures gives a lower bound of the membrane stretching modulus $k_{\text{stretch}}=\tau/\alpha\geqslant140$ erg/cm^2. The pressure range is too low to completely avoid the entropic term; this is the reason for the lower bound. To our knowledge, this is the first measure of the stretching modulus of the mixed-(charged/neutral) phospholipid membrane in ionic solution. It is comparable to similar measurements on other phospholipids under different solution conditions [39,5].

IV. DISCUSSION

The shape assumed by a vesicle with microtubules inside depends on its size, the rate at which microtubules nucleate, and its membrane tension. Vesicle size determines (a) the length of microtubule that can interact forcefully with the membrane, and (b) the number of microtubules that can reach that length before significantly depleting the available supply of tubulin. For example, a vesicle of 1-μm diameter with 30-μM tubulin would have tubulin enough for only 6-μm worth of microtubule. A microtubule 1 μm long would lower the tubulin concentration 17%, thereby significantly inhibiting the nucleation of other microtubules [15] and enhancing its own inherent instability [14]. In our experiments, vesicles were ~10 μm in diameter, and the enclosed concentration was sufficient to create millimeters of microtubule.

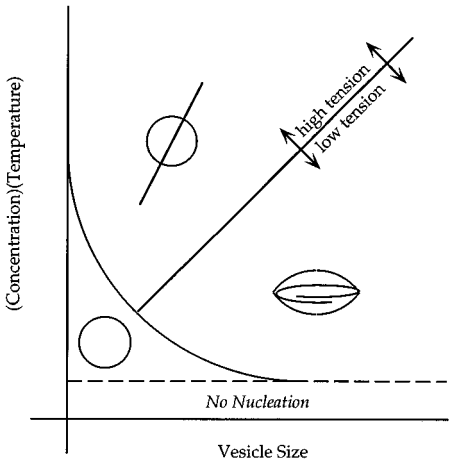

FIG. 13. Sketch of shape space of vesicles with microtubules inside. Under conditions of low concentration and/or low temperature, there is no spontaneous nucleation of microtubules. When nucleation does occur, small-sized vesicles continue to be unaffected by microtubules because the finite supply of tubulin is insufficient to support growth. At high tubulin concentration or temperature or large vesicle volume, this constraint is overcome. The vesicles are then ϕ shaped if (a) the microtubules are able to interact with the membrane while they are short and resistant to buckling, or (b) they nucleate in large numbers and interact with the membrane collectively; otherwise, the vesicles are discoid shaped. Tension of the membrane shifts the boundary between these regimes: higher tension increases the range of the discoid shape, and lower tension increases that of the ϕ shape.

Nucleation rate determines the number of microtubules that form. At a high nucleation rate, many microtubules form at once, they span the vesicle diameter, and form a rigid bundle. At a low nucleation rate, they arrive individually at the vesicle size, and buckle one after the other.

Membrane tension determines the work required to distort the membrane. At low tension, distortions damp curvature fluctuations excited by thermal energy, k_BT. At high tension (e.g., under osmotic stress), curvature fluctuations are already damped, and distortion requires actually stretching the membrane, at an energetic cost of $\sim10^7k_BT/\mu$m^2. In our experiments, membrane tension was controlled with micropipet aspiration.

A sketch of the shape space is shown in Fig. 13. The ϕ shape occurs when conditions favor the microtubule: at high tubulin concentrations and temperatures, where nucleation is rapid, and in small vesicles, where the microtubules are relatively strong (Fig. 13). The discoid shape occurs at the opposite extreme, when nucleation is slow and the vesicle is large and/or taut. Then the microtubules reach the vesicle diameter one by one, buckle readily, and grow along a curve tangent to the membrane. Bent microtubules align if they can exaggerate one circumference of the vesicle but, with their ends out of register, they cannot collectively straighten.

For the phospholipid combination and solution conditions used here, measurements of membrane elasticity were not possible without microtubules. Charged vesicles with excess membrane area (i.e., osmotically compressed) that are unsupported by microtubules tend to internalize pockets of the surrounding fluid. Aspiration measurements on such empty vesicles were frustrated by a slow drift of the membrane into

the pipet ($\sim$1 μm/min), perhaps due to the release of these inclusions. Aspiration measurements on vesicles with many microtubules were stable, however. Presumably, membrane tension generated by the microtubules prevents the formation of inclusions.

The charge repulsion between DOPS headgroups promotes the formation of unilamellar vesicles. The membrane stretching modulus is proportional to the number of bilayers, and our measurement is consistent with what might be expected of a single bilayer for such long-chain lipids [28]. Also, vesicles which appeared diffuse under the microscope were selected against on the presumption that charge repulsion between bilayers was the reason for this appearance. The sedimentation was effective in clearing away the vesicles which did not entrap a tubulin-containing medium.

Unlike other techniques, micropipet aspiration enables measurement of bundles containing hundreds of microtubules. The collective strength of a bundle, be it linear or circular, is consistent with the sum of the strengths of the individual microtubules. Were there a strong lateral attraction between microtubules, they would essentially fuse along their lengths, and the bending rigidity would depend on the square of their number. This was not observed. The consistency of the results for different geometries and total lengths indicates a classical elastic response for microtubules. This is in contrast to the findings of a recent study using a method based on optical tweezers, where it was found that the bending rigidity was itself a function of microtubule length [34]. In the case of a ϕ shape, the membrane deformation increases the bundle's resistance to collapse under loads beyond critical buckling.

V. CONCLUSION

Micropipet aspiration applied to vesicles containing microtubules has yielded a measurement of microtubule bending stiffness in the range of published values obtained by different methods (Sec. III B), and a measurement of the membrane stretching modulus consistent with published values obtained for membranes of different composition under different ionic conditions (Sec. III D). It has also revealed a qualitative organization of vesicle shape (Fig. 13).

Microtubules in vesicles capture two fundamental structural themes found in eukaryotic cells. Bundles are most common. They are found in the axons of nerve cells [8], in cilia and flagella [40], and in the stalks of hair cells [41], for example. Bands are more specialized. They are a defining characteristic of amphibian and avian red blood cells, for example [42,7]. Such cell shapes are known to be directly influenced by microtubules [43,44].

It is, of course, naïve to expect that the microtubule geometries measured in this experiment are an accurate model of the ones found *in vivo*. Associated proteins (e.g., MAP2, tau) or motor proteins (e.g., dynein, kinesin) may create lateral interactions between microtubules *in vivo* [45]. Furthermore, microtubules *in vivo* are typically anchored to organizing centers (e.g., centrosomes, axonemes). One might find increased biological relevance by repeating this work on microtubules with associated proteins, motor proteins or organizing centers also in the vesicles [46].

ACKNOWLEDGMENTS

This work was supported in part by the National Science Foundation under Grant No. Phy-9408905.

[1] Phospholipids are amphiphilic molecules which spontaneously organize into bimolecular sheets. The hydrophobic alkyl chains of the molecules are sandwiched between two layers of hydrophilic phosphate head groups. The structure is impermeable to most molecules, with the notable exception of water [permeability coefficient k $H_2O\sim5$ $\mu m3/\mu m^2$ s, T. E. Thompson and C. Huang, Ann. N.Y. Acad. Sci. **137**, 740 (1966)].

[2] A. D. Bangham and R. W. Horne, J. Mol. Biol. **8**, 660 (1964).

[3] R. B. Gennis, *Biomembranes* (Springer-Verlag, New York, 1989).

[4] The membrane can exist in both a fluid and a gel-like state, but the latter is not found in living systems. A collection of studies on the physical properties of membranes is contained in Structure and Conformation of Amphiphilic Membranes, edited by R. Lipowsky, D. Richter, and K. Kremer (Springer-Verlag, Berlin, 1992).

[5] J. F. Faucon, M. D. Mitov, P. Méléard, I. Bivas, and P. Bothorel, J. Phys. (Paris) **50**, 2389 (1989).

[6] M. Kirschner and T. Mitchison, Cell **45**, 329 (1986).

[7] B. Winckler and F. Solomon, Proc. Natl. Acad. Sci. U.S.A. **88**, 6033 (1991).

[8] F. Lafont, M. Rouget, A. Rousselet, C. Valenza, and A. Prochiantz, J. Cell Sci. **104**, 433 (1993).

[9] R. Kwok and E. Evans, Biophys. J. **35**, 637 (1981).

[10] H. Hotani and H. Miyamoto, Adv. Biophys. **26**, 135 (1990).

[11] M. Elbaum, D. Kuchnir Fygenson, and A. Libchaber Phys. Rev. Lett. **76**, 4078 (1996).

[12] 200-ml lipid:chloroform solution at 25-mg lipid/ml chloroform was deposited on 1-cm^2 teflon squares. After evaporation, the dry lipid was resuspended in 3 ml of buffer. These quantities are not critical. It is essential that all materials be clean and free of surfactants, which can contaminate the lipids. One major source of contamination can be the oil from the dessicator vacuum pump. It is best to pump quickly and seal the dessicator rather than pump continuously. It is also important to control the time and temperature in the oven because of heat-induced degradation of the lipid.

[13] R. C. Williams, Jr. and J. C. Lee, Meth. Enzym. **85**, 376 (1982).

[14] D. Kuchnir Fygenson, E. Braun, and A. Libchaber, Phys. Rev. E **50**, 1579 (1994).

[15] D. Kuchnir Fygenson, H. Flyvbjerg, K. Sneppen, A. Libchaber, and S. Leibler, Phys. Rev. E **51**, 5058 (1995).

[16] U. Pick, Arch. Biochem. Biophys. **212**, 186 (1981).

[17] Osmotic considerations are subtle here. Pipes is a diacid requiring 1.5 positive counterions to bring it to a pH of 6.8. Thus 100-mM Pipes at pH 6.8 has the same osmolarity as 250 mM of simple, nondissociating solute.

[18] It is important to pump thoroughly on the mineral oil to draw out its lighter components which might contaminate the vesicles.

[19] The micropipet is mounted horizontally under the stereoscope. A looped filament of tantalum wire, 0.5-mm diameter, connected to a variable transformer, is mounted independently. A small glass bead, deposited on the filament, melts when current is turned on. If the bead is brought to touch the tip immediately after shutting off the current, the thermal shock will cleave the tip cleanly at the point of contact. The size of the final tip can be selected to within a micrometer by the color and intensity of the light refracted by it.

[20] That the membrane is never punctured by the microtubules is apparent from (a) the fact that the tubulin-free environment outside the vesicles would force the microtubules to depolymerize and (b) straight microtubules buckle under increased membrane tension (see Secs. III B–III D).

[21] Note that the microtubule radius (12.5 nm) is much smaller than the typical vesicle radius (5 μm).

[22] D. Kuchnir Fygenson, M. Betterton, J. Marko, and A. Libchaber (unpublished).

[23] Assuming the (spontaneously nucleated) microtubules are 14 dimers around, and given that a tubulin dimer is 4×8 nm, with its long axis aligned with the microtubule.

[24] Estimated values range from $2k_BT$ to $10k_BT$, as derived from measurements of the critical concentration for microtubule assembly [D. Dreschel *et al.*, Mol. Biol. Cell **3**, 1141 (1992); R. Walker *et al.*, J. Cell Biol. **107**, 1437 (1988)].

[25] This is not to imply that there were no other microtubules in the vesicle, but that only one of them was long enough to deform the vesicle forciably. This was clear from careful visualization, as the temperature decreased and the microtubules inside slowly disappeared.

[26] Typical microtubule growth rates for 25-μM tubulin at 27 °C are $\sim$4 μm/min (see Ref. [14]). Thus in 10 s the microtubule might increase by at most $\sim$0.5 μm, or $\sim$5%.

[27] This condition is maintained by the high concentration of salts (buffer) inside the vesicle, which creates a large osmotic pressure in response to any change in volume.

[28] W. Helfrich and R.-M. Servuss, Nuovo Cimento D **3**, 137 (1984).

[29] E. Evans and W. Rawicz, Phys. Rev. Lett. **64**, 2094 (1990).

[30] L. D. Landau and E. M. Lifshitz, *Statistical Physics* (Pergamon, Oxford, 1980), p. 396.

[31] S. Yamazaki, T. Maeda, and T. Miki-Nomura, in *Biological Functions of Microtubules and Related Structures*, edited by H. Sakai, H. Mohri, and G. G. Borisy (Academic, New York, 1982), p. 41.

[32] F. Gittes, B. Mickey, J. Nettleton, and J. Howard, J. Cell Biol. **120**, 923 (1993).

[33] P. Venier, A. C. Maggs, M.-F. Carlier, and D. Pantaloni, J. Biol. Chem. **269**, 13353 (1994).

[34] M. Kurachi, M. Hoshi, and H. Tashiro, Cell Motil. Cytoskel. **30**, 221 (1995).

[35] B. Mickey and J. Howard, J. Cell Biol. **130**, 909 (1995).

[36] This concentration is 20% higher than the one in which the vesicles were frozen or thawed, due to osmotic crushing in the sample cell.

[37] Since the microtubule length appeared stable, this concentration was taken to be at the transition for unbounded growth.

[38] L. D. Landau and E. M. Lifshitz, *Theory of Elasticity* (Pergamon, Oxford, 1980), p. 533.

[39] E. Evans and D. Needham, J. Phys. Chem. **91**, 4219 (1987).

[40] K. M. Yamada, B. S. Spooner, and N. K. Wessells, Proc. Natl. Acad. Sci. U.S.A. **66**, 1206 (1970).

[41] S. Kamimura and K. Takahashi, Nature **293**, 566 (1981).

[42] J. B. Tucker, C. C. Paton, C. G. Henderson, and M. M. Mogensen, Cell Motil. Cytoskel. **25**, 49 (1993).

[43] S. Kim, M. Magendantz, W. Katz, and F. Solomon, J. Cell Biol. **104**, 51 (1987).

[44] J. R. Jacobs and J. K. Stevens, J. Cell Biol. **103**, 907 (1986).

[45] J. Knops, K. S. Kosik, G. Lee, J. D. Pardee, L. Cohen-Gould, and L. McConlogue, J. Cell Biol. **114**, 725 (1991).

[46] G. W. Brodland and R. Gordon, J. Biomech. Eng. **112**, 319 (1990).